J Intell Robot Syst (2017) 87:211–229
DOI 10.1007/s10846-017-0502-0

Inverse Kinematics and Workspace Analysis of a 3 DOF Flexible Parallel Humanoid Neck Robot

Bingtuan Gao · Zhenyu Zhu · Jianguo Zhao · Leijie Jiang

Received: 12 September 2015 / Accepted: 26 January 2017 / Published online: 2 March 2017

Abstract To mimic the human neck's three degree-of-freedom (DOF) rotation motion, we present a novel bio-inspired cable driven parallel robot with a flexible spine. Although there exists many parallel robotic platform that can mimic the human neck motion, most of them have only two DOF, with the yaw motion being actuated separately. The presented flexible parallel humanoid neck robot employs a column compression spring as the main body of cervical vertebra and four cables as neck muscles to connect the base and moving platform. The pitch and roll movements of moving platform are realized by the two dimensional lateral bending motion of the flexible spring, and a bearing located at the top of the compression spring and embedded in the moving platform is used to achieve the yaw motion of the moving platform. By combing the force and torque balance equations with the lateral bending statics of the spring, inverse kinematics and optimizing the cable placements to minimize the actuating cable force are investigated. Moreover, the translational workspace corresponding to pitch and roll movements and rotational workspace corresponding to yaw movement are analyzed with positive cable tension constraint. Extensive simulations were performed and demonstrated the feasibility and effectiveness of the proposed inverse kinematics and workspace analysis of the novel 3 DOF flexible parallel humanoid neck robot.

Keywords Humanoid neck · Flexible parallel robot · Kinematics · Optimal design · Workspace

1 Introduction

With the development of robotic industry, the design and manufacture of robots become increasingly highly personified. Among them, humanoid neck robot is an important part of the body of a highly personified robot. Humanoid neck robot can be roughly divided into serial type and parallel type [1]. Serial humanoid neck robot often uses chain structure, and each joint can be controlled separately [2–4], while parallel neck robot usually contains a fixed base and a moving platform which connected to trunk and head respectively, actuated by some parallel controllers between them [5, 6]. For serial robot, it has an advantage of simple structure and control, with a large workspace. However,

The work is financial supported by National Science Foundation of China (11102039), the Excellent Young Teachers Programm of Southeast University (2242015R30024), and Six Talent Peaks Project of Jiangsu Province (2014-ZBZZ-001).

B. Gao (✉) · Z. Zhu · L. Jiang
School of Electrical Engineering, Southeast University, Nanjing, China
e-mail: gaobingtuan@seu.edu.cn

J. Zhao
Department of Mechanical Engineering, Colorado State University, Fort Collins, CO, USA

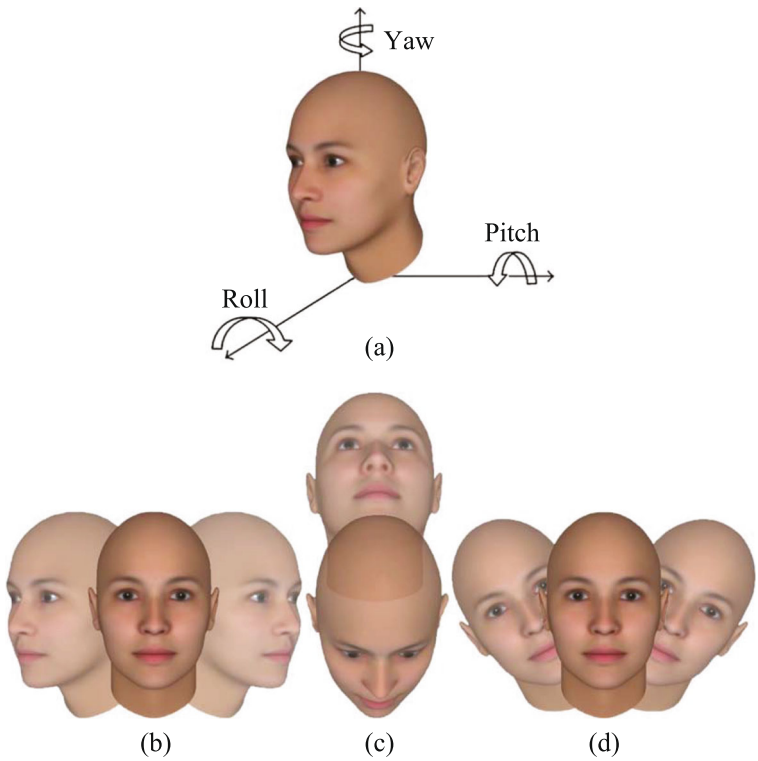

Fig. 1 (**a**) Illustration of 3-DOF human head movements (**b**)Yaw (**c**)Pitch (**d**)Roll

the advantages of parallel robot are rarely cumulative error, good dynamic response and large carrying capacity [7].

Most parallel humanoid neck robots install actuators inside them, resulting in high motion noise. However, real human neck will not produce noise in the movement. In some specific occasions, such as the ordnance noise research shown in [8] which requires a low motion noise humanoid neck robot, flexible humanoid neck structure was preferred to reduce motion noise in order to meet the acoustic requirement. Flexible parallel humanoid neck robot is possible to achieve the three degree of freedom (DOF) motion, namely yaw, pitch and roll as shown in Fig. 1, through reasonable structure design. One can summarize the requirements of the flexible parallel humanoid neck robot in the following. First, it should be able to imitate all the 3-DOF movements of real person's neck. Second, the robot should not make noises itself during motions to be able to work in mute environments. To achieve above requirements, one should also consider the size of actuators to reduce the cost and space, which means optimize design of the robot. Therefore, it is necessary to establish and solve its kinematic model, to obtain its inverse position and forces of flexible part, and then optimal the size of actuators.

To meet the listed two key requirements, a cable-driven humanoid neck robot with a flexible spring spine has been proposed in our previous work [8, 9]. However, this parallel mechanism can only realize 2-DOF head motion, namely pitch and roll. To realize yaw motion, another revolute joint is needed. Using four cables to realize 2-DOF rotating movements of the humanoid robotic neck is redundant, which increases the cost. Consequently, a similar 2-DOF humanoid parallel robot driven by three cables is proposed and analyzed in [10]. Nonetheless, the above humanoid parallel robot can only realize 2-DOF rotating movements by itself. By analyzing existing 2-DOF robot and human anatomical structure, we proposed a novel robot which can accomplish 3-DOF rotating movements with its flexible parallel structure, as shown in Fig. 2. Compared with the previous

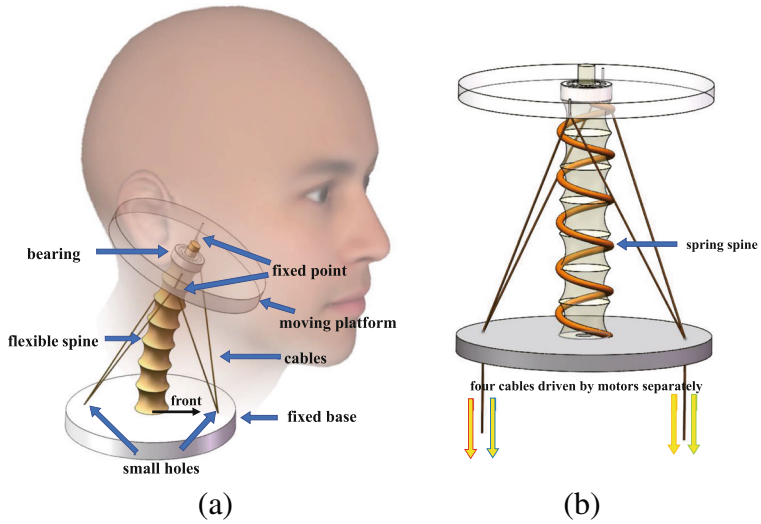

Fig. 2 Overview of the robot design

humanoid parallel robotic necks [8, 10], the unique feature of the proposed robot is that 3-DOF rotating movements of the platform can be realized by controlling four driving cables directly.

To analyze and control of the flexible parallel robot, kinematics of the parallel robot should be studied at first. Compared with serial robot, the inverse kinematics of parallel robot are more complex and developed later [1]. During the process of solving inverse kinematics, motion equations are usually nonlinear and transcendental [11]. As a result, it is difficult to solve them directly. Traditional methods of solving inverse kinematics include numerical method, analytic method, and geometric method [12, 13]. For numerical method, the advantage is that it can obtain the approximate solutions of certain accuracy while the exact solutions of complex actual problem cannot be found out [13, 14]. Analytic method uses a set of analytical expressions, eliminating unknowns except the input and output, and then makes it become a one element higher order equation for solution [15–18]. Although one can obtain an accurate solution, the mathematical deduction process is very complicated, and it is too slow to solve those equations when the index of unknown is higher than 4. Geometric method solve the inverse kinematic problems through geometrical relationship in the robot structure. This kind of method is very intuitional and avoid the huge amount of computation in analytic method [19–21]. Beside the traditional methods mentioned above, some scholars use improved genetic algorithm, which can acquire good robustness and global convergence [22, 23]. Also, quaternion and dual-quaternion method are used to express rotational motion more uniform and effective [24, 25]. Neural network method has faster speed and better accuracy [26]. Since each of these methods has advantages and disadvantages, some scholars use them in combination to improve accuracy and efficiency for better solutions [27].

Although different aforementioned techniques of solving inverse kinematics of parallel robot have been studied and developed, few research was done for inverse kinematics of cable-driven parallel robot with a spring spine. Appropriate modeling of the flexible spring spine in the parallel robot is the key for the overall inverse kinematics. There are mainly two types of lateral bending models of the compression spring in literature. The first one takes lateral bending motion of the spring as a circular arc of a circle; therefore, homogeneous transformation matrix of the robot can be calculated based on geometry, which leads to solving inverse kinematics directly [6]. The second one takes lateral bending of the spring as a linear two-order differential equation; therefore, inverse kinematics of the robot has be combined with the linear two-order differential equation of the spring spine for possible solutions [9, 10]. These two modeling methods for the spring spine were compared in the our

previous work [28]. By studying the forces in the cables, we found out that negative cable force exists in the first geometric method when the bending amplitude increases, which contradicts with that cables can only generate one direction pulling force. Therefore, the geometric method used in [6] is inaccurate for the overall kinematics calculation. As a result, the differential equation method to analyze the spring spine will also be employed in this paper. Once the inverse kinematics is solved together with the linear differential equation of the spring spine, optimal design and workspace analysis of the novel 3-DOF flexible parallel humanoid neck robot will be presented in this paper. And main contributions can be summarized as follows.

- A novel compact cable-driven parallel robot with flexible spring spine is proposed to mimic 3-DOF rotating movements of human neck.
- Inverse kinematics of the robot is solved together with linear differential equation for bending motion of the spring spine.
- Quantitative analyses on kinematics, optimal design, and workspace of the parallel humanoid neck robot are presented.

The rest of the paper is organized as follows: In Section 2, we describe the robot and establish its inverse kinematics model by statics balance. After that, we solve the inverse position and simulate the cable lengths and forces in Section 3. And then we discuss the optimal design, translational workspace and rotational workspace of the robot in Section 4. Finally, Section 5 concludes the paper.

2 Inverse Kinematics of Flexible Parallel Humanoid Neck Robot

2.1 Mechanism Description

As we can see in Fig. 2, the mechanism is composed of a fixed base and a moving platform, which is connected to human trunk and head respectively. The fixed base and moving platform are connected by a flexible spine and four cables. The flexible spine's bottom is fixed with the base while the top is connected with the moving platform through a bearing,

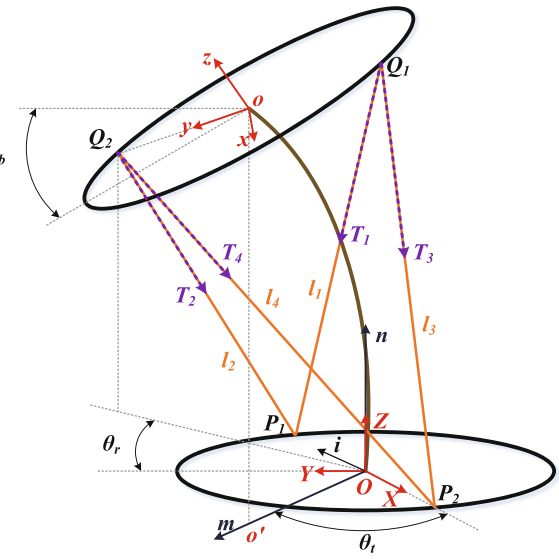

Fig. 3 Schematic of the mechanism model

which makes the moving platform become rotational. A compression spring is used as the flexible spine. The mechanism is actuated by the four cables between two platforms. The top of these cables are fixed with the moving platform two by two and distributed in 180 degrees. The bottom of these cables pass through the holes in the base, actuated by four drivers separately. The holes in the base are also distributed in 180 degrees. In the initial state, the line connected two fixed points on the moving platform is perpendicular to the line connected two holes in the base.

We establish the model of the mechanism, shown in Fig. 3. The mechanism is divided into four parts as follows:

- Fixed base
  The fixed base is a part, which connected to the trunk of the mechanism. We define a base coordinate frame $OXYZ$ on the base. The thickness of the base is ignored. The origin of the frame is at the center of the base, the OX axis is along OP_2, the OY axis is perpendicular to OP_2. We determine the OZ axis by right-hand rule.
- Moving platform
  The moving platform is the part connected to the head on which a moving coordinate frame $oxyz$ is defined. The thickness of the moving platform

is also ignored. The origin of the frame is at the center of the moving platform. The ox axis is perpendicular to OQ_2, the oy axis is along OQ_2, and the oz axis is determined by right-hand rule.

– Cables
Four cables fixed at Q_i, pass through P_i, are pulled to actuate the mechanism. The mass, diameter and elasticity are ignored. The correspondence of four cables and the points on platforms are shown in figure [3-1], which is l_1 to P_1Q_1, l_2 to P_1Q_2, l_3 to P_2Q_1, l_4 to P_2Q_2. And the radius of the two platforms are $|OP_i| = p\,(i = 1, 2)|OQ_i| = q\,(i = 1, 2)$ respectively. We denote T_i $(i = 1, 2, 3, 4)$ as the forces in cable l_i $(i = 1, 2, 3, 4)$,$\mathbf{v}_i$ $(i = 1, 2, 3, 4)$ as the unit vector along the direction of cable l_i $(i = 1, 2, 3, 4)$. In this paper, vectors are used bold letters to denote (e.g. $\mathbf{T}_i = T_i\mathbf{v}_i$).
– Spring
The spring connects the center of the moving platform and the base, providing force and torque to support the mechanism motion. It cannot move in radial direction but can buckle in axial direction due to a fixed connection with the base. As a result, the spring can be considered as a curve, which links O and o. The tangent line at O is perpendicular to the base plane and the tangent line at o is perpendicular to the moving platform plane. Due to the existence of a bearing, we can suppose that the radial rotational movement is realized by the bearing. Also, the torsional strength of the compression spring is quite large, so we consider it would not twist and bend in a plane. That is to say, the spring itself cannot rotate about the oz axis.

The mechanism realizes the yaw motion by the bearing on the top of the spring, which is in the position of o. At the same time, four stayed-cables provide the actuated forces in sideways to make the moving platforms rotate. This is quite different from the three cable driven parallel mechanism, which only has straight pulling force and cannot rotate about the oz axis.

We conclude the assumptions mentioned above as follows:

– **Assumption 1**: Ignore the thickness of fixed base and moving platform, and consider them as two disks. Ignore the mass, diameter and elasticity of the four cables. Ignore the shape and radius of the compression spring when analyze the statics of the mechanism.
– **Assumption 2**: The rotation about oz axis is realized through the bearing, and the spring cannot rotate, so it bend in a plane.

We can see from Fig. 3, when the spring bends, o' is the vertical projection of o on the fixed base. So the spring curve is in the plane Ooo'. To describe the bending spring, we establish a planar coordinate frame Omn attached to Ooo'. The origin of the frame is coincide with O, the origin of the base frame. The Om axis is along Oo' axis, the On axis is along OZ axis. On the premise of **Assumption 1** and **Assumption 2**, we need five parameters to describe the position of the moving platform:

– θ_m: the angle between Om axis and OX axis (describe the bending direction of the spring).
– θ_b: the angle between fixed base's plane and moving platform's plane (describe the bending range of the spring).
– n_0: the length between o' and o in the frame Omn (describe the vertical height of the bending spring).
– m_0: the length between o' and O in the frame Omn (describe the vertical projection of the bending spring on the fixed base).
– θ_r: the anticlockwise rotation angle of the moving platform through the bearing (describe the yaw angle of the humanoid neck).

There are other ways to set the parameters to describe the position of the moving platform, but the above five parameters are the most appropriate. However, the five parameters are not all independent, so we cannot assign the values of the parameters arbitrarily. In fact, there are only four independent parameters among them. To facilitate the calculation behind, we consider m_0 as the dependent parameter. That is to say, m_0 can be determined by other four parameters.

For ease of coordinate transformation, we use homogeneous coordinate to describe P_i on the fixed base with respect to $OXYZ$:

$${}^{O}\mathbf{p}_1 = (-p, 0, 0, 1)^{\mathrm{T}},\ {}^{O}\mathbf{p}_2 = (p, 0, 0, 1)^{\mathrm{T}}$$

Similarly, the homogeneous coordinate of Q_i in the moving platform with respect to $oxyz$ are:

$${}^{o}\mathbf{q}_1 = (0, -q, 0, 1)^{\mathrm{T}},\ {}^{o}\mathbf{q}_2 = (0, q, 0, 1)^{\mathrm{T}}$$

We need to convert moving coordinate to base coordinate to do unified operation, so we need to obtain the rotational matrix from the moving frame to the base frame. We can divide the transformation into two steps to obtain the matrix more conveniently.

First, the base coordinate frame should rotate about the axis i, which is perpendicular to the Omn plane, with an angle θ_b. Second, rotate with an angle θ_r about the rotated oz axis. Third, a translational transformation should be taken.

Using Rodrigues' formula, the transformation matrix of the first step can be obtained as:

$$\mathbf{R} = e^{\hat{\mathbf{i}}\theta_b} = \mathbf{I} + \hat{\mathbf{i}}\sin\theta_b + \hat{\mathbf{i}}^2(1-\cos\theta_b) = \begin{bmatrix} s_{110} & s_{120} & s_{130} \\ s_{210} & s_{220} & s_{230} \\ s_{310} & s_{320} & s_{330} \end{bmatrix}$$

$$\begin{aligned} s_{110} &= \sin^2\theta_m + \cos\theta_b\cos^2\theta_m \\ s_{120} &= t_{210} = (\cos\theta_b - 1)\cos\theta_m \sin\theta_m \\ s_{130} &= -t_{310} = \sin\theta_b \cos\theta_m \\ s_{230} &= -t_{320} = \sin\theta_b \sin\theta_m \\ s_{220} &= \cos^2\theta_m + \cos\theta_b\sin^2\theta_m \\ s_{330} &= \cos\theta_b \end{aligned}$$

where $\mathbf{i} = [-\sin\theta_m, \cos\theta_m, 0]^{\mathrm{T}}$, so its skew symmetric matrix is:

$$\hat{\mathbf{i}} = \begin{bmatrix} 0 & 0 & \cos\theta_m \\ 0 & 0 & \sin\theta_m \\ -\cos\theta_m & -\sin\theta_m & 0 \end{bmatrix}$$

One can obtain the homogeneous form of $\mathbf{R}$:

$$\mathbf{R}_h = \begin{bmatrix} s_{110} & s_{120} & s_{130} & 0 \\ s_{210} & s_{220} & s_{230} & 0 \\ s_{310} & s_{320} & s_{330} & 0 \\ 0 & 0 & 0 & 1 \end{bmatrix}$$

Then, the transformation matrix of the second step is:

$$\mathbf{M}_{rot\_oz} = \begin{bmatrix} \cos\theta_r & -\sin\theta_r & 0 & 0 \\ \sin\theta_r & \cos\theta_r & 0 & 0 \\ 0 & 0 & 1 & 0 \\ 0 & 0 & 0 & 1 \end{bmatrix}$$

The translational matrix can be written as:

$$\mathbf{M}_{trans} = \begin{bmatrix} 1 & 0 & 0 & a \\ 0 & 1 & 0 & b \\ 0 & 0 & 1 & c \\ 0 & 0 & 0 & 1 \end{bmatrix}$$

Using reverse multiplication principle of coordinate transformation, we can obtain the final rotational matrix from moving frame to base frame by reverse multiplying the three matrix above:

$${}^{O}\mathbf{T}_o = \mathbf{M}_{trans}\mathbf{M}_{rot\_oz}\mathbf{R}_h = \begin{bmatrix} s_{11} & s_{12} & s_{13} & m_0\cos\theta_m \\ s_{21} & s_{22} & s_{23} & m_0\sin\theta_m \\ s_{31} & s_{32} & s_{33} & n_0 \\ 0 & 0 & 0 & 1 \end{bmatrix}$$

$$\begin{aligned} s_{11} &= \cos\theta_r(\sin^2\theta_m + \cos\theta_b\cos^2\theta_m) \\ &\quad + \sin\theta_r(\cos\theta_b - 1)\cos\theta_m\sin\theta_m \\ s_{12} &= \cos\theta_r(\cos\theta_b - 1)\cos\theta_m\sin\theta_m \\ &\quad + \sin\theta_r(\cos^2\theta_m + \cos\theta_b\sin^2\theta_m) \\ s_{13} &= \cos\theta_r\sin\theta_b\cos\theta_m + \sin\theta_r\sin\theta_b\sin\theta_m \\ s_{21} &= -\sin\theta_r(\sin^2\theta_m + \cos\theta_b\cos^2\theta_m) \\ &\quad + \cos\theta_r(\cos\theta_b - 1)\cos\theta_m\sin\theta_m \\ s_{22} &= -\sin\theta_r(\cos\theta_b - 1)\cos\theta_m\sin\theta_m \\ &\quad + \cos\theta_r(\cos^2\theta_m + \cos\theta_b\sin^2\theta_m) \\ s_{23} &= -\sin\theta_r\sin\theta_b\cos\theta_m + \cos\theta_r\sin\theta_b\sin\theta_m \\ s_{31} &= -\sin\theta_b\cos\theta_m \\ s_{32} &= -\sin\theta_b\sin\theta_m \\ s_{33} &= \cos\theta_b \end{aligned}$$

2.2 Inverse Kinematics and Statics

We must obtain the cable length in order to control the robot. This lead to inverse kinematics analyze to the robot, and solve its inverse position. The key is statics analysis.

Let $\mathbf{x} = [\theta_m, \theta_b, \theta_r, n_0]^{\mathrm{T}} \in \mathbf{R}^4$,the unsolved cable lengths $\mathbf{l} = [l_1, l_2, l_3, l_4]^{\mathrm{T}} \in \mathbf{R}^4$, so the relationship between them can be written as:

$$\mathbf{l} = f(\mathbf{x}),\ f : \mathbf{R}^4 \to \mathbf{R}^4$$

We can determine ${}^{O}\mathbf{T}_o$ completely if we obtain the dependent parameter m_0 by using independent variable $\mathbf{x}$. Therefore, l_i can be solved by the following formula:

$$l_i = ||{}^{O}\mathbf{T}_o{}^{o}\mathbf{q}_{i_1} - {}^{O}\mathbf{p}_{i_2}||,\ (i_1 = 1, 2;\ i_2 = 1, 2)$$

However, m_0 is depend on the mechanical and geometrical characteristics of the mechanism. In other words, m_0 comes from the lateral bending of the spring, which caused by the cable pulling and gravity of the head. So we will analyze the statics of the mechanism to solve m_0 in the following steps:

– Transform all the cable forces and torques at the center of the moving platform, and consider the resultant force and torque to establish the balance equations.

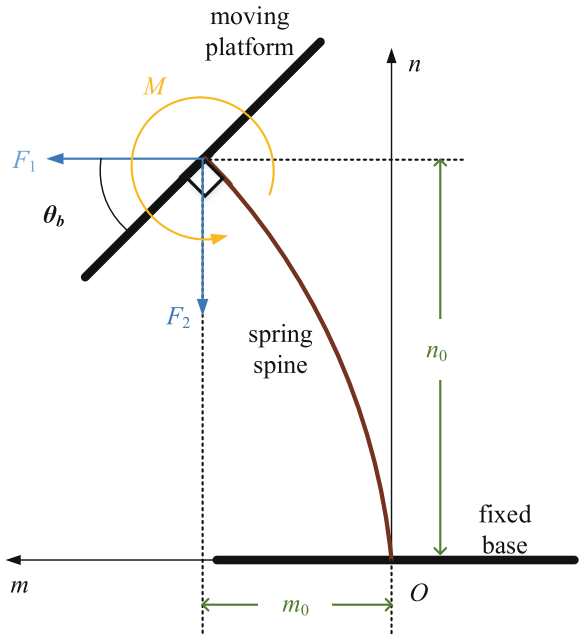

Fig. 4 Force and torque analysis

- Using the resultant force and torque to establish the spring's lateral bending equations.
- Solve m_0 from equations above.
- Obtain ${}^{O}\mathbf{T}_o$, cable lengths and cable forces.

These steps will be amplified in the ensuring paragraphs.

According to **Assumption 2**, the resultant force and torque can be transformed in the plane Omn, or the spring does not bending in the plane. In addition, when the spring is treated as a curve, forces at the center of the moving platform can be regarded at the top of the spring. The statics analysis is shown in Fig. 4. We convert the resultant force into two perpendicular forces F_1 and F_2. F_1 is horizontal and F_2 is vertical. M is the resultant torque, it is perpendicular to the plane Omn inward. We make the third assumption as:

- **Assumption 3**: Regardless of the mass of the head and treat the moving platform as a mass point m at the center of the spring.

We have the following equations by the force and torque balance:

$$\sum_{i=1}^{4} \mathbf{T}_i + \mathbf{F} = \mathbf{0} \tag{1}$$

$$\sum_{i=1}^{4} {}^{O}\mathbf{r}_i \times \mathbf{T}_i + \mathbf{M} = \mathbf{0} \tag{2}$$

where

$$\mathbf{T}_i = T_i {}^{O}\mathbf{v}_i$$
$$\mathbf{F} = [-F_1 \cos\theta_m, -F_1 \sin\theta_m, F_2 - mg]^{\mathrm{T}}$$
$$\mathbf{M} = [M \sin\theta_m, -M \cos\theta_m, 0]^{\mathrm{T}}$$

From (1) and (2), we have:

$$\sum_{i=1}^{4} T_i {}^{O}\mathbf{v}_i + [-F_1 \cos\theta_m, -F_1 \sin\theta_m, F_2 - mg]^{\mathrm{T}} = \mathbf{0} \tag{3}$$

$$\sum_{i=1}^{4} {}^{o}\mathbf{r}_i \times T_i {}^{O}\mathbf{v}_i + [M \sin\theta_m, -M \cos\theta_m, 0]^{\mathrm{T}} = \mathbf{0} \tag{4}$$

where ${}^{O}\mathbf{v}_i = ({}^{O}\mathbf{p}_i - {}^{O}\mathbf{T}_o {}^{o}\mathbf{q}_i)/||{}^{O}\mathbf{p}_i - {}^{O}\mathbf{T}_o {}^{o}\mathbf{q}_i||, {}^{O}\mathbf{r}_i$ corresponds to $\overrightarrow{oQ_i}$ in the base frame:

$${}^{O}\mathbf{r}_1 = q[-s_{12}, -s_{22}, -s_{32}]^{\mathrm{T}}, \; {}^{O}\mathbf{r}_2 = q[s_{12}, s_{22}, s_{32}]^{\mathrm{T}}$$

$${}^{O}\mathbf{r}_3 = q[-s_{12}, -s_{22}, -s_{32}]^{\mathrm{T}}, \; {}^{O}\mathbf{r}_4 = q[s_{12}, s_{22}, s_{32}]^{\mathrm{T}}$$

We did not consider the rotational angle θ_r about the oz axis, the following is the explanation. The forces lead to the rotation of the moving platform must be the component forces tangent to the side of the moving platform plane. When the robot moves to the final position, the moving platform must remain stationary with balanced forces or it will go on rotating. Therefore, the resultant torque composed by the rotational component forces must be 0. Besides, each arm of component force is equal to the radius of the moving platform, so the rotational resultant force must be 0 too. That is to say, there is no need to write the equation of this DOF.

Six equations set can be obtained from Eqs. 3 and 4:

$$s_0 \cos\theta_s T'_{1\Sigma} + (a + bt_{12})(T'_2 - T'_3) + (a - bt_{12}) \times (T'_1 - T'_4) + F_1 \cos\theta_s = 0 \tag{5}$$

$$s_0 \sin\theta_s T'_{1\Sigma} + bt_{22} T'_{2\Sigma} + F_1 \sin\theta_s = 0 \tag{6}$$

$$t_0 T'_{1\Sigma} + bt_{32} T'_{2\Sigma} - F' = 0 \tag{7}$$

$$-T'_{1\Sigma}(t_0 t_{22} - s_0 t_{32} \sin\theta_s) + \frac{M}{b} \sin\theta_s = 0 \tag{8}$$

$$T'_{2\Sigma}(t_0 t_{12} - s_0 t_{32} \cos\theta_s) - T'_{2\Sigma} a t_{32} - \frac{M}{b} \cos\theta_s = 0 \tag{9}$$

$$-T'_{2\Sigma}(s_0 t_{12} \sin\theta_s - s_0 t_{22} \cos\theta_s) + T'_{2\Sigma} a t_{22} = 0 \tag{10}$$

where:

$T_i' = T_i/l_i$
$F_2' = F_2 - mg$
$T_{1\Sigma}' = T_1' + T_2' + T_3' + T_4'$
$T_{2\Sigma}' = T_2' + T_4' - T_1' - T_3'$

We can rewrite it into a matrix form:

$$\mathbf{PT} = \mathbf{F} \tag{11}$$

where:

$\mathbf{F} = \left[F_1 \cos\theta_m,\ F_1 \sin\theta_m, -F_2',\ \frac{M}{q}\sin\theta_m, -\frac{M}{q}\cos\theta_m,\ 0\right]^{\mathrm{T}}$
$\mathbf{T} = \left[T_1', T_2', T_3', T_4'\right]^{\mathrm{T}}$
$\mathbf{P} = \begin{bmatrix} p_{11} & p_{12} & p_{13} & p_{14} \\ p_{21} & p_{22} & p_{23} & p_{24} \\ p_{31} & p_{32} & p_{33} & p_{34} \\ p_{41} & p_{42} & p_{43} & p_{44} \\ p_{51} & p_{52} & p_{53} & p_{54} \\ p_{61} & p_{62} & p_{63} & p_{64} \end{bmatrix}$

$p_{11} = p - qs_{12} + m_0\cos\theta_m$
$p_{12} = p + qs_{12} + m_0\cos\theta_m$
$p_{13} = -p - qs_{12} + m_0\cos\theta_m$
$p_{14} = -p + qs_{12} + m_0\cos\theta_m$
$p_{21} = -qs_{22} + m_0\sin\theta_m$
$p_{22} = qs_{22} + m_0\sin\theta_m$
$p_{23} = -qs_{22} + m_0\sin\theta_m$
$p_{24} = qs_{22} + m_0\sin\theta_m$
$p_{31} = n_0 - qs_{32}$
$p_{32} = n_0 + qs_{32}$
$p_{33} = n_0 - qs_{32}$
$p_{34} = n_0 + qs_{32}$
$p_{41} = n_0 s_{22} - m_0 s_{32}\sin\theta_m$
$p_{42} = -t_0 s_{22} + m_0 s_{32}\sin\theta_m$
$p_{43} = n_0 s_{22} - m_0 s_{32}\sin\theta_m$
$p_{44} = -n_0 s_{22} + m_0 s_{32}\sin\theta_m$
$p_{51} = -n_0 s_{12} + ps_{32} + m_0 s_{32}\cos\theta_m$
$p_{52} = n_0 s_{12} - ps_{32} - m_0 s_{32}\cos\theta_m$
$p_{53} = -n_0 s_{12} - ps_{32} + m_0 s_{32}\cos\theta_m$
$p_{54} = n_0 s_{12} + ps_{32} - m_0 s_{32}\cos\theta_m$
$p_{61} = -ps_{22} - m_0 s_{22}\cos\theta_m + m_0 s_{12}\sin\theta_m$
$p_{62} = ps_{22} + m_0 s_{22}\cos\theta_m - m_0 s_{12}\sin\theta_m$
$p_{63} = ps_{22} - m_0 s_{22}\cos\theta_m + m_0 s_{12}\sin\theta_m$
$p_{64} = -ps_{22} + m_0 s_{22}\cos\theta_m - m_0 s_{12}\sin\theta_m$

We use Mathematica to calculate the rank of the augmented matrix [**P**, **F**], and the result is 5. That is to say, there exist one dependent equation among the equation set. After seeking, Eq. 8 is the dependent one.

Until now, we have 8 unknowns but only 5 independent equations, so we need to find other equations to solve the unknowns. We focus on the lateral bending spring. In [9], the spring was treated as a spring bar to investigate its bending characteristics, so we have the following equation for every cross section of the spring:

$$\beta\frac{\mathrm{d}^2 m/\mathrm{d}n^2}{\left[1+(\mathrm{d}m/\mathrm{d}n)^2\right]^{3/2}} = M + F_2(m_0 - m) + F_1(n_0 - n) \tag{12}$$

where n_0 is the vertical height of the spring after compression, β is the flexural rigidity after compression when the spring is treated as a solid bar. If β_0 is the flexural rigidity before compression, l_0 is the initial length of the spring, we have:

$$\beta = \beta_0\frac{n_0}{l_0}$$

We also consider a bending angle no more than 15 degrees for an healthy individual, so the Eq. 12 can be simplified due to [9], we have:

$$F_1 = X_1 m_0 + Y_1 \tag{13}$$

$$M = X_2 m_0 + Y_2 \tag{14}$$

where:

$X_1 = -\frac{a_2c_1 - a_1c_2}{a_2b_1 - a_1b_2}, Y_1 = -\frac{a_2d_1 - a_1d_2}{a_2b_1 - a_1b_2}$

$X_2 = -\frac{b_2c_1 - b_1c_2}{b_2a_1 - b_1a_2}, Y_2 = -\frac{b_2d_1 - b_1d_2}{b_2a_1 - b_1a_2}$

$a_1 = 1 - \cos(\sqrt{F_2/\beta}n_0)$
$b_1 = \sqrt{\beta/F_2}\sin(\sqrt{F_2/\beta}n_0) - n_0\cos(\sqrt{F_2/\beta}n_0)$
$c_1 = -F_2\cos(\sqrt{F_2/\beta}n_0)$
$d_1 = 0$
$a_2 = \sqrt{F_2/\beta}\sin(\sqrt{F_2/\beta}n_0)$
$b_2 = \cos(\sqrt{F_2/\beta}n_0) + n_0\sqrt{F_2/\beta}\sin(\sqrt{F_2/\beta}n_0) - 1$
$c_2 = F_2\sqrt{F_2/\beta}\sin(\sqrt{F_2/\beta}n_0)$
$d_2 = -F_2\tan\theta_b$

In fact, the spring length usually decrease after compression. The length reduction caused by lateral buckling can be neglected according to [10] and [9]. Therefore, we can use Hooke's law to obtain F_2 approximately:

$$F_2 = K(l_0 - n_0) \tag{15}$$

Table 1 Parameters of the mechanism

p(m)	q(m)	n_0(m)	m(kg)
0.06	0.06	0.085	0.05

Combine Eqs. 13–15 with balance Eqs. 5–7, 9, 10, we have an 8-equation set about 8 unknowns as follows:

$$s_0 \cos\theta_s T'_{1\Sigma} + (a + bt_{12})(T'_2 - T'_3)$$
$$+(a - bt_{12})(T'_1 - T'_4) + F_1 \cos\theta_s = 0 \quad (16)$$
$$s_0 \sin\theta_s T'_{1\Sigma} + bt_{22} T'_{2\Sigma} + F_1 \sin\theta_s = 0 \quad (17)$$
$$t_0 T'_{1\Sigma} + bt_{32} T'_{2\Sigma} - F' = 0 \quad (18)$$
$$T'_{2\Sigma}(t_0 t_{12} - s_0 t_{32}\cos\theta_s) - T'_{2\Sigma} a t_{32} - \frac{M}{b}\cos\theta_s = 0 \quad (19)$$
$$-T'_{2\Sigma}(s_0 t_{12}\sin\theta_s - s_0 t_{22}\cos\theta_s) + T'_{2\Sigma} a t_{22} = 0 \quad (20)$$
$$K(l_0 - n_0) = F_2 \quad (21)$$
$$X_1 m_0 + Y_1 = F_1 \quad (22)$$
$$X_2 m_0 + Y_2 = M \quad (23)$$

The above eight equations can be proved independent, so we can find out a unique solution from the equation set.

3 Inverse Kinematics Simulation

Based on the Inverse-kinematics equation set, we obtain the inverse position and cable forces in Matlab. Table 1 shows the parameters we choose:

The compression spring's parameters are in Table 2,where G is the shearing modulus, E is the elastic modulus, r is the radius, d is the diameter of the spring wire, K is the spring constant. Therefore, we can get β_0 from the Eqs. 24 and 25:

$$I = \frac{\pi d^4}{64} = 9.811 \times 10^{-12}(\mathrm{m}^4) \quad (24)$$

$$\beta_0 = \frac{2EGIh_0}{\pi r(E + 2G)} = 0.2321 \quad (25)$$

3.1 The Effect of θ_m and θ_b to Cable Lengths and Forces

We let $\theta_r = 0$ due to that we only consider the effect of θ_m and θ_b to cable lengths and forces. θ_m is varied from 0 to 2π and θ_b is varied from 0 to $\pi/9$. The result is shown in Fig. 5, and the z coordinate shows the cable lengths and cable forces separately.

We can observe from Fig. 5 that T_i increase with θ_b. In other words, the more the spring bends, the more cable forces are needed. We also observe that each cable length has the same range, so is each cable force. We can imagine that when the humanoid neck does not rotate about oz axis, 4 cable lengths and forces must have the same range with each other. We also discover that T_1 and T_2, T_3 and T_4 are symmetrical about $\theta_m = \pi$. This because the whole mechanism is symmetrical about the oOX plane when it does not rotate about oz axis. The above observations can be comprehended more clearly in Fig. 6. Figure 6 is a cross section of Fig. 5 at $\theta_p = \pi/9$.

3.2 The Effect of θ_r to Cable Lengths and Forces

We consider $\theta_r \neq 0$ next, let $\theta_r = \pi/6$, $\theta_b \in (0, \pi/9)$, $\theta_m \in (0, 2\pi)$, we have Fig. 7.

Comparing Fig. 5 with Fig. 7, we discover that l_1, l_4 get longer while l_2, l_3 get shorter when the humanoid neck rotate about oz axis clockwise. To have an observation more clearly, we plot the figure when $\theta_r = \pi/6$, $\theta_b = \pi/9$, $\theta_m \in (0, 2\pi)$, shown in Fig. 8. Comparing Fig. 8 with Fig. 6, as a result of the clockwise angle θ_r, the range of l_1 and l_4 changes from (0.11, 0.135) to (0.12, 0.15) approximately, and the range of l_2 and l_3 changes from (0.11, 0.135) to (0.095, 0.115) approximately. We can imagine the change intuitively.

Table 2 Parameters of the compression spring

l_0(m)	h_0(m)	G(GPa)	E(GPa)	r(m)	d(m)	K(N/m)
0.1016	0.0195	81.2	196.5	22.73×10^{-3}	3.76×10^{-3}	4153

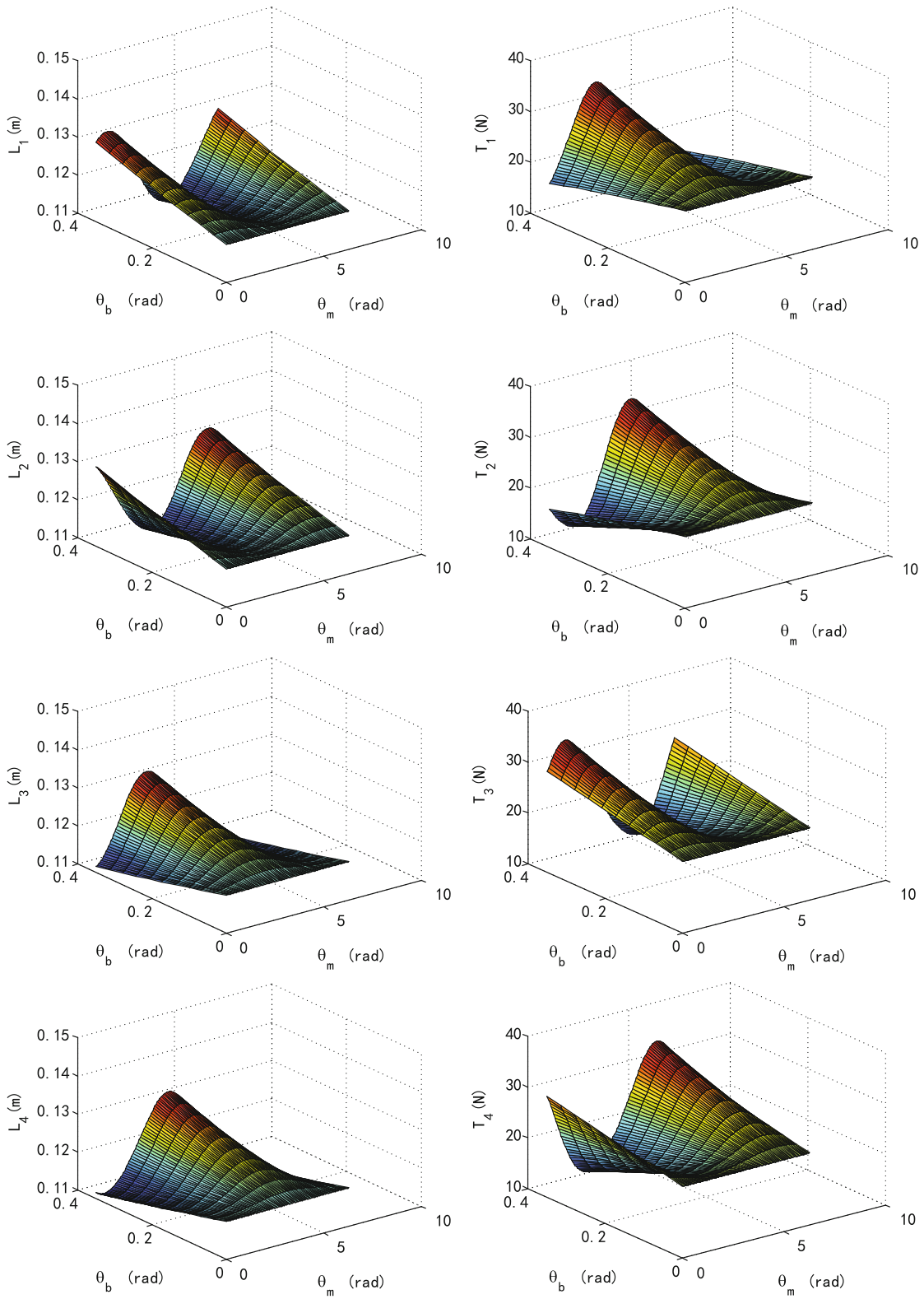

Fig. 5 Cable lengths and forces when $\theta_r = 0\ \theta_m, \in (0, 2\pi), \theta_b \in (0, \frac{\pi}{9})$

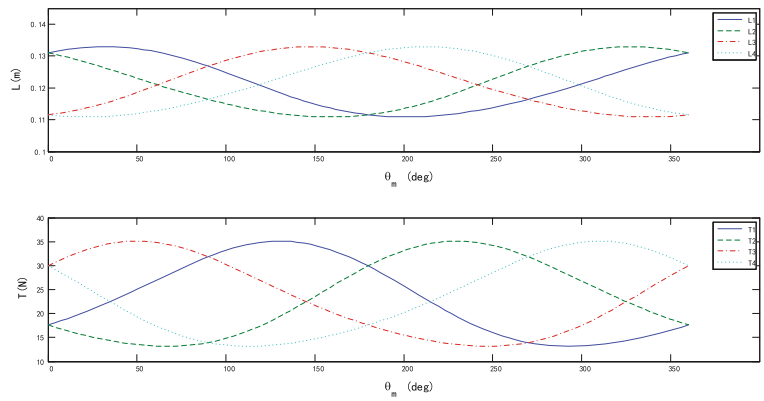

Fig. 6 Cable lengths and forces when $\theta_r = 0$, $\theta_m \in (0, 2\pi)$, $\theta_b = \frac{\pi}{9}$

However, the change trend of cable forces are on the contrary. Cable lengths and forces satisfy the negative correlation in [10].

Let $\theta_b = \pi/9$, $\theta_r \in (0, \pi/6)$, $\theta_m \in (0, 2\pi)$ to analyze the cable lengths and forces when it comes to a fixed θ_b with variable θ_r and θ_m. The result is shown in Fig. 9.

When θ_b is a certain value, cable lengths and forces change sinusoidally. We can imagine that when the humanoid neck only has a rotational motion, cable must change sinusoidally, which can be observed more clearly from Figs. 10 and 11.

Last but not least, compared with the three-cable driven humanoid neck in [10] and [9], the cable lengths are not symmetric with cable forces because of an additional degree of freedom θ_r.

4 Optimal Design and Workspace Analysis

4.1 Optimal Design

We need to optimize the cable forces to reduce the size of actuators. When the final position is certain, θ_m, θ_b, θ_r, t_0 is also determined, and F_1, F_2, M_1, m_0 can be worked out too. The parameters can be changed are only p and q, which is the end position of the four cables. We will use the numerical method to obtain the optimal p and q in the following.

We use $\mathbf{t} = [t_1, t_2, t_3, t_4]^{\mathrm{T}}$ to express all the cable forces. Two norms are used to define the measure [9, 10] as follows:

$$2-\text{norm}: T_2 = \sqrt{\sum_{i=1}^{4} t_i^2}$$

$$\infty-\text{norm}: T_\infty = \max\{t_1, t_2, t_3, t_4\}$$

Due to that cables cannot produce nonnegative forces, we ignored absolute value symbols in the above definition. T_2 snd T_∞ are functions of $\theta_m, \theta_b, \theta_r, n_0, p$ snd q, because t_i can be solved by Eqs. 16–23. Different n_0 can be obtained by changing the pretightening four cables, so we let $n_0 = 0.085m$ without loss of generality. However, it is very difficult to solve the optimal problem by analytical method because the expressions of two norms are quite complex. Therefore, we decide to use numerical method to solve the problem.

We can transform the optimal problem into:

$$\text{minimize } \Omega(p, q)$$

where $\Omega(p, q) = \{T_{2\ or\ \infty}(p, q) | \theta_m, \theta_b, \theta_r, n_0, p, q\}$ both have a upper bound and lower bound limited by physiology. At the same time, cables forces cannot be negative. The optimal result can be expressed as:

$$\Omega^* = \Omega(p^*, q^*) = \min_{p,q}\{\Omega(p, q)\}$$

where * means the optimal value of the function.

We choose workspace V as the optimal space, so the target function can be defined as:

$$\Omega_{\max}(p, q) = \max_{V} T_{2\ or\ \infty} = \max_{V} \lambda(\theta_m, \theta_b, \theta_r, p, q)$$

This target function λ indicates the minimum power of actuators, which determine the size of them. In humanoid robotics, it is necessary to reduce the size of actuators.

The results from different measures and initial values are shown in Table 1. We can see that different initial values have the same result when using same measures, but different measures lead to different optimal results. To verify the optimal results, we plot the 3D graphs of $\Omega_{\max}(p, q)$ in Fig. 12.

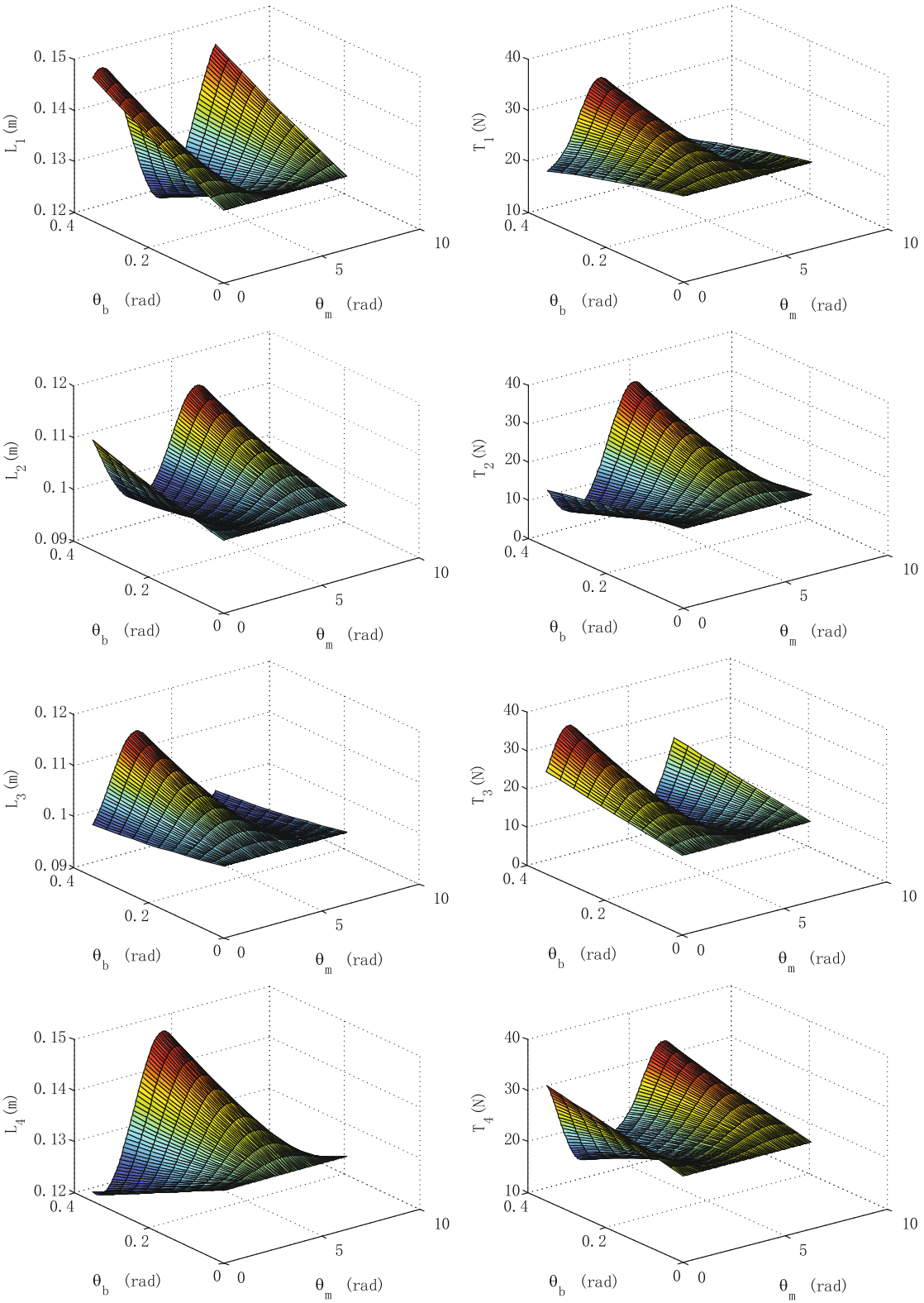

Fig. 7 Cable lengths and forces when $\theta_r = \frac{\pi}{6}, \theta_m \in (0, 2\pi), \theta_b \in (0, \frac{\pi}{9})$

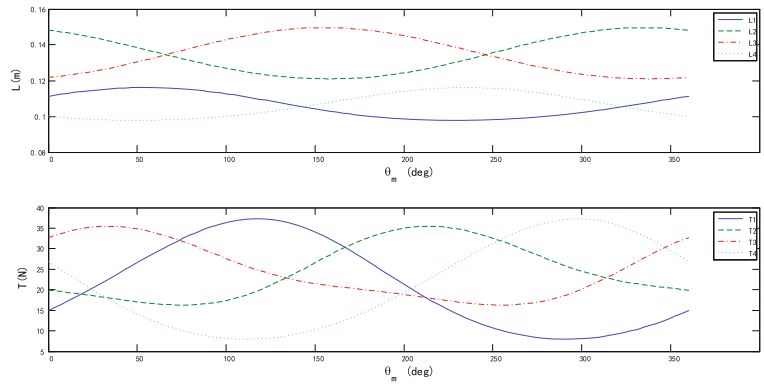

Fig. 8 Cable lengths and forces when $\theta_r = \frac{\pi}{6}$, $\theta_m \in (0, 2\pi)$, $\theta_b = \frac{\pi}{9}$

From the figure, we can see that $\Omega_{\max}(p, q)$ measured by T_2 has an area of the same color around the optimal point (0.0638, 0.0619). Also, people usually tend to use $\infty-$norm to measure this target function. So we choose (0.0800, 0.0795) as the optimal point.

4.2 Workspace Analysis

The workspace of a cable driven flexible parallel robot is the space which cables can constrain the moving platform with nonnegative forces regardless of any external torque [9].

In this paper, humanoid neck mechanism can realize yaw, pitch and roll motions. However, yaw motion only happens in the plane of moving platform, so it does not affect the translational workspace. Therefore, we discuss the two kind of workspace separately: the translational workspace, which is determined by θ_m and θ_b; and the rotational workspace, which is determined by θ_r.

4.2.1 Translational Workspace

In this condition, we don't need to consider the effect of rotational angle θ_r. Therefore, let $\theta_r = 0$. We consider the translational workspace is the space which the center of the moving platform can approach. Denote all the cable forces and forces on the moving platform as torque vector $\mathbf{w}$, $\mathbf{w} = -[\mathbf{F}, \mathbf{M}]^{\mathrm{T}}$, so the balance equation of forces and torques can be written as:

$$\begin{bmatrix} {}^{O}\mathbf{v}_1 & {}^{O}\mathbf{v}_2 & {}^{O}\mathbf{v}_3 & {}^{O}\mathbf{v}_4 \\ {}^{O}\mathbf{r}_1 \times {}^{O}\mathbf{v}_1 & {}^{O}\mathbf{r}_2 \times {}^{O}\mathbf{v}_2 & {}^{O}\mathbf{r}_3 \times {}^{O}\mathbf{v}_3 & {}^{O}\mathbf{r}_4 \times {}^{O}\mathbf{v}_4 \end{bmatrix} \begin{bmatrix} t_1 \\ t_2 \\ t_3 \\ t_4 \end{bmatrix} = \mathbf{w} \tag{26}$$

Suppose that $\kappa_i = [{}^{O}\mathbf{v}_i, {}^{O}\mathbf{r}_i \times {}^{O}\mathbf{v}_i]^{\mathrm{T}}$ is the vector determined by the ith cable, and the Eq. 26 can be written as:

$$\mathbf{At} = \mathbf{w} \tag{27}$$

where $\mathbf{A} = [\kappa_1, \kappa_2, \kappa_3, \kappa_4]$, $\mathbf{t} = [t_1, t_2, t_3, t_4]^{\mathrm{T}}$. $\mathbf{A}$ is called structure matrix, it highly depend on the structure of the whole mechanism and the position of the moving platform.

If the moving platform lies in the translational workspace, the following request must be satisfied:

$$\begin{cases} \mathrm{Rank}(\mathbf{A}) = 4 \\ \mathbf{t} > 0 \end{cases} \tag{28}$$

According to Eq. 28, we can discretize a certain space around the initial position of the moving platform into discrete points, and judge each point whether satisfy Eq. 28 or not. If a point satisfy Eq. 28, it is in the workspace and keep it, else it is not in the workspace and drop it. All the reserved points compose the workspace.

We discretize the space $x \in (-0.03, 0.03)$, $y \in (-0.03, 0.03)$, $z \in (0.08, 0.1)$ at certain steps, and set $p = 0.08m$, $q = 0.0795m$ from the optimal result. The translational workspace is shown in Fig. 13. From the figure, we can see that the translational workspace is like a cone, similar to the workspace in [9].

4.2.2 Rotational Workspace

When θ_b and θ_m has arrived at a terminal position, θ_r can still rotate in a certain range. This range is called

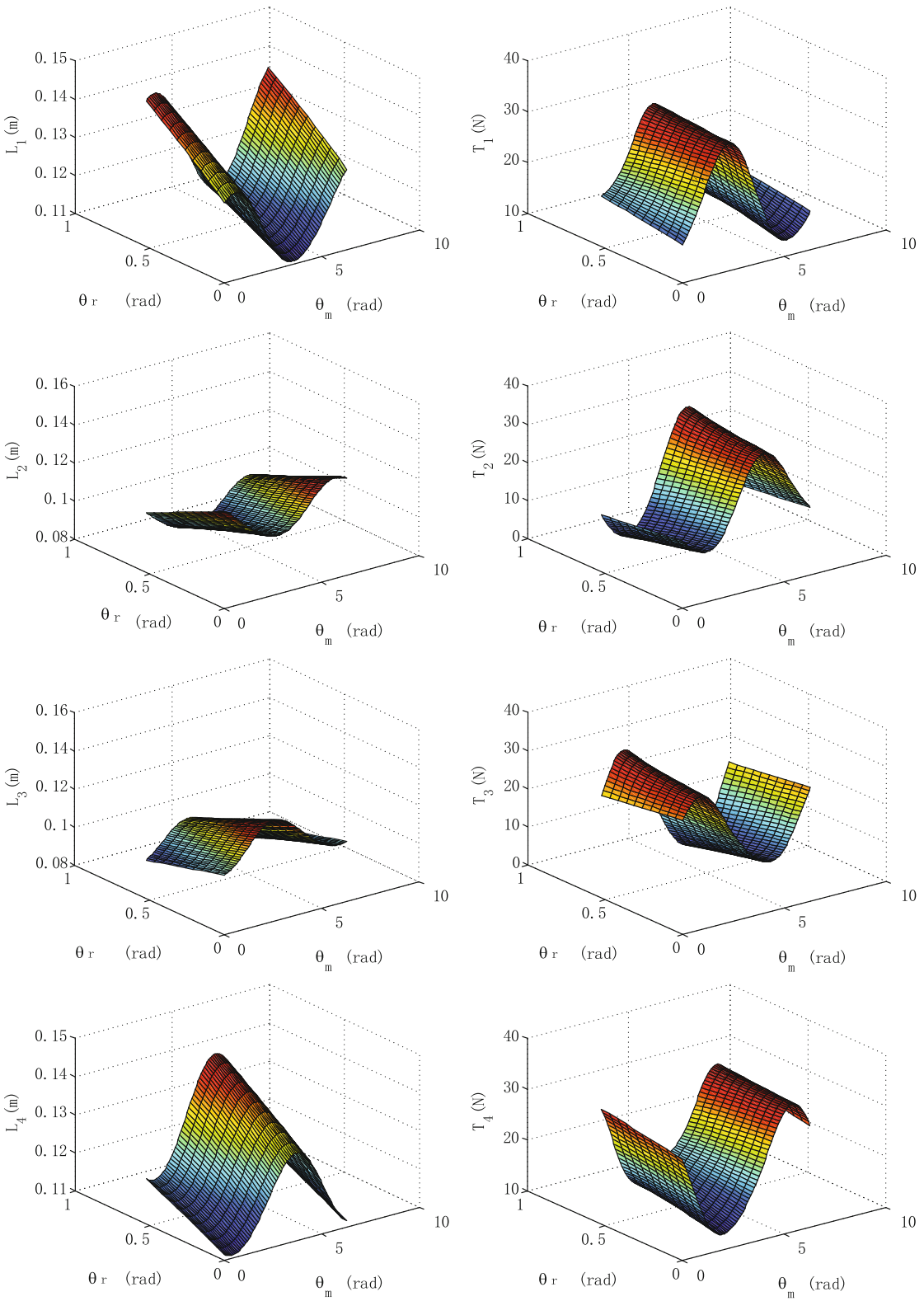

Fig. 9 Cable lengths and forces when $\theta_b = \frac{\pi}{9}$, $\theta_r \in (0, \frac{\pi}{6})$, $\theta_m \in (0, 2\pi)$

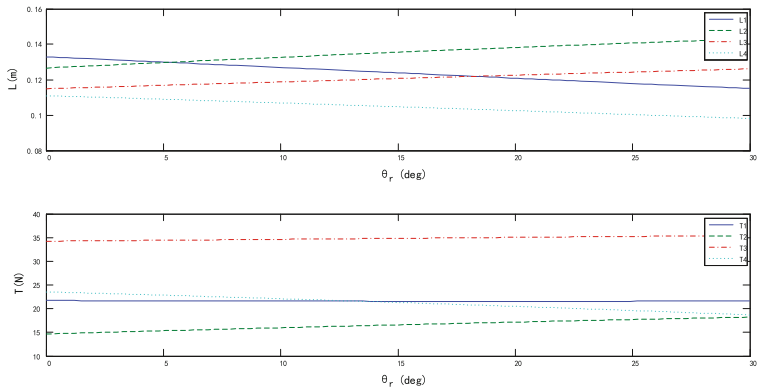

Fig. 10 Cable lengths and forces when $\theta_b = \frac{\pi}{9}$, $\theta_r \in (0, \frac{\pi}{6})$, $\theta_m = \frac{\pi}{6}$

rotational workspace D. Not hard to imagine that each pair of θ_b and θ_m can determine a range of θ_r. Denote the mapping relationship as σ, we have:

$$D(\theta_r) = \sigma(\theta_m, \theta_b)$$

The constraint condition of rotational workspace is same as Eq. 28, and the deterministic process is similar too. The difference is the rotational workspace must be consecutive. Therefore, once upon a breakpoint appears, the following points in the range are no need to be judged anymore.

According to the above method, we choose $p = 0.03$ m, $q = 0.08$ m and n_0 is obtained by pretightening the cables. Without loss of generality, let $n_0 = 0.085$ m. The rotational workspace is shown in Fig. 14. The rotational workspace is between the two surfaces, which correlated stronger with θ_m than that with θ_b. The workspace is central symmetry about the point $\theta_r = 0$, $\theta_m = 180°$ at a certain θ_b, which correspond with our intuitive feeling.

Figures 15 and 16 is the rotational workspace when $p = 0.08$ m, $q = 0.08$m and $p = 0.08$ m, $q = 0.03$ m, respectively. We can discover that the volume of rotational workspace has a relationship with the value of p/q, the workspace when $p/q = 8/3 \approx 2.667$ and $p/q = 3/8 = 0.375$ is smaller than that when $p/q = 8/8 = 1$. That is to say, the rotational workspace increases when p/q get closer to 1.

From the above analysis of rotational workspace, the p/q of the optimal result ($p = 0.08$ m, $q = 0.0795$ m) is slightly larger than 1. Therefore, the rotational workspace can be approximately biggest when the cable forces are optimized. The anatomical structure of human neck does have $p/q > 1$ [9]. During the long evolutionary history of human, neck structure has considered both the smallest actuated forces and the biggest rotational workspace. This also proves the result of our analysis.

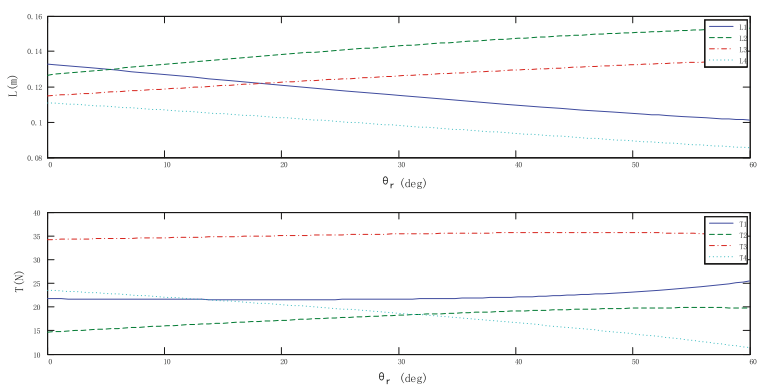

Fig. 11 Cable lengths and forces when $\theta_b = \frac{\pi}{9}$, $\theta_r \in (0, \frac{\pi}{6})$, $\theta_m = \frac{\pi}{3}$

Fig. 12 The 3D graphs of $\Omega_{\max}(p, q)$

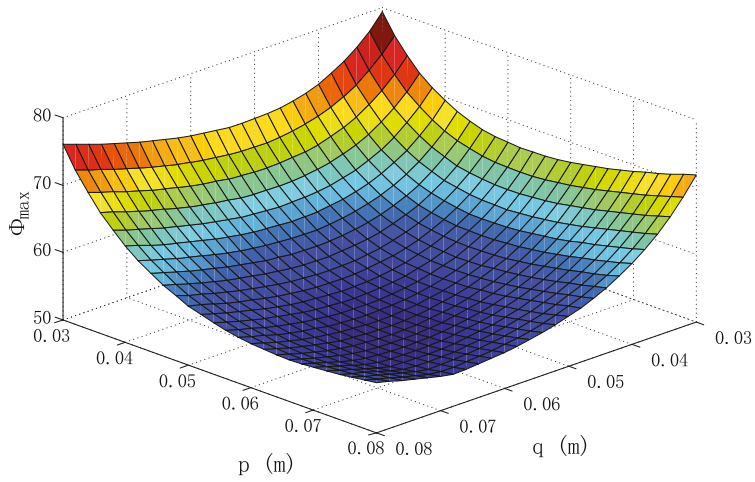

(a) 2-norm

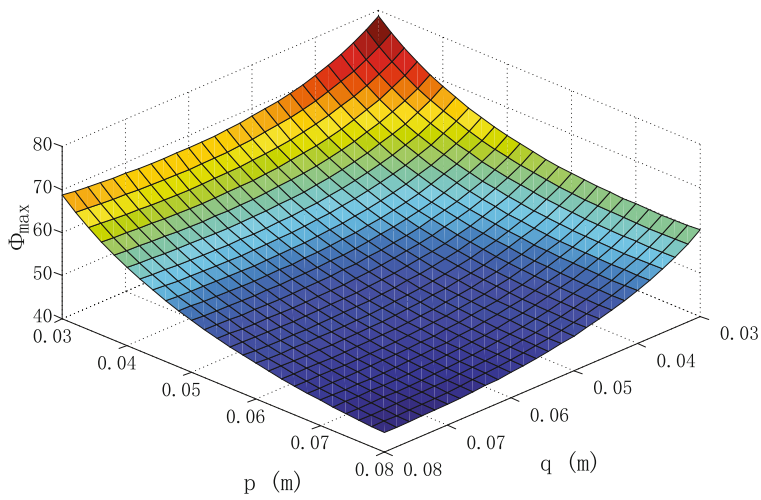

(b) ∞-norm

5 Conclusions

This paper presents a novel bio-inspired 3 DOF flexible parallel humanoid neck robot driven by 4 cables. Inverse kinematics, optimizing the cable displacement and workspace of the robot are analyzed and simulated based on Matlab. It is shown that the inverse kinematics of the flexible parallel robot has to be solved by combing the force and torque balance equations with the lateral bending statics of the flexible spine. According to the simulation results on minimizing design for actuating cable force, it's better to place the end position of each cables near the upper bound. And the simulation results on workspace analysis show that the translational workspace corresponding to pitch and roll movements is an inverted cone and the rotational workspace corresponding to yaw movement increases as the connecting radii of the driving cables to the base and to the moving platform getting closer. The modeling and analysis method presented in this paper for the novel cable-driven flexible parallel robot can be extended to other cable-driven parallel robots with a flexible spine.

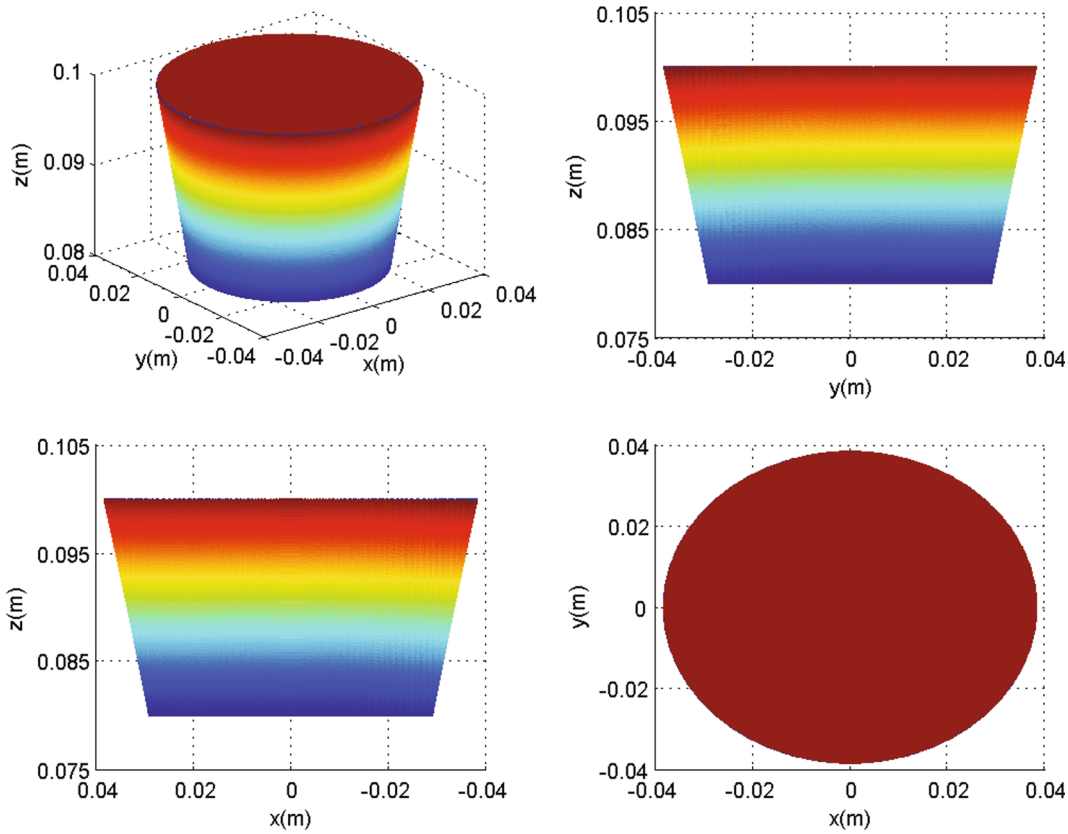

Fig. 13 Translational workspace

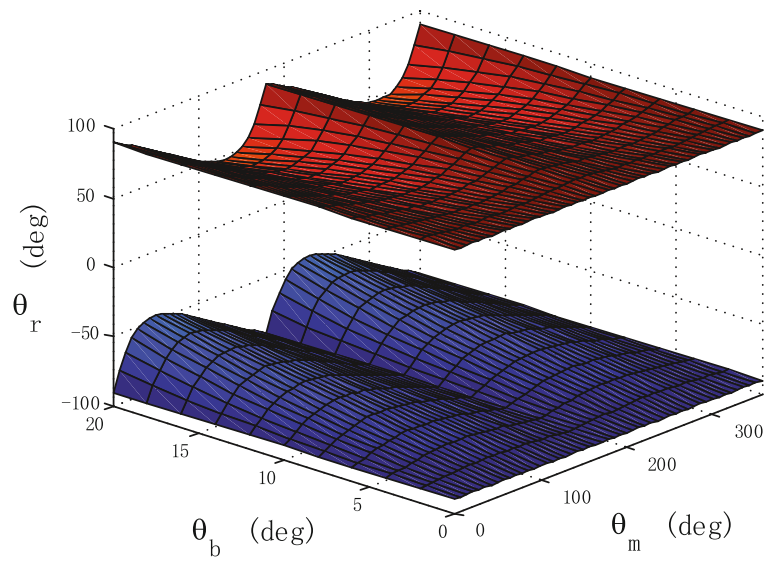

Fig. 14 Rotational workspace when $p = 0.03$m, $q = 0.08$m

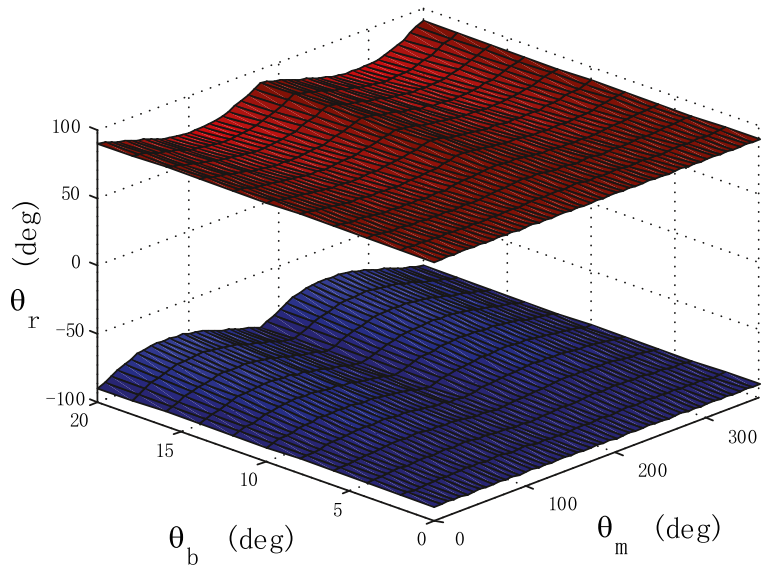

Fig. 15 Rotational workspace when $p = 0.08$m, $q = 0.08$m

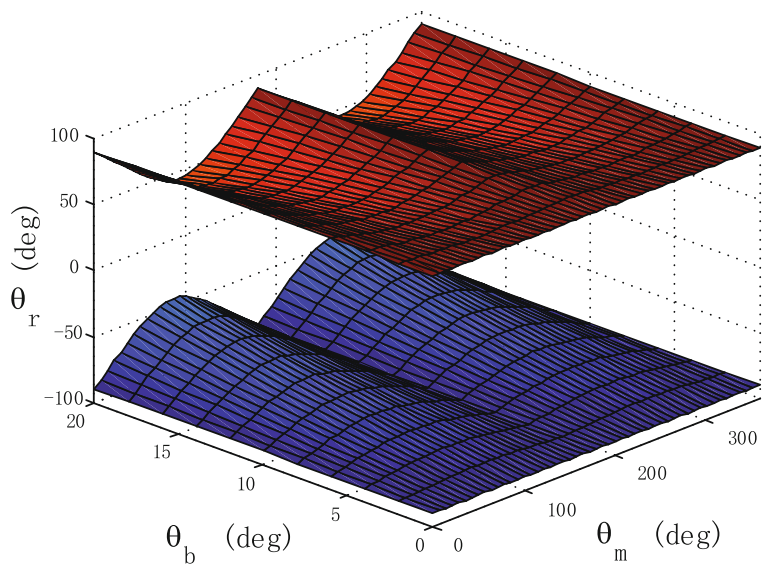

Fig. 16 Rotational workspace when $p = 0.08$m, $q = 0.03$m

References

1. Merlet, J.-P. Parallel Robots, 2nd edn. Springer, Netherlands (2006)
2. Park, I.W., Kim, J.Y., Cho, B.K., Oh, J.H.: Control hardware integration of a biped humanoid robot with an android head. Robot. Auton. Syst. **56**(1), 95–103 (2008)
3. Beira, R., Lopes, M., Praca, M., Santos-Victor, J., Bernardino, A., Metta, G., Becchi, F., Saltaren, R.J.: Design of the robot-Cub (iCub) head. In: Proceeding of IEEE International Conference on Robotics and Automation, Orlando, FL, pp. 94–100 (2006)
4. Albers, A., Brudniok, S., Ottnad, J., Sauter, C., Sedchaicham, K.: Upper body of a new humanoid robot the design of ARMAR III. In: Proceeding of IEEE/RAS International Conference on Humanoid Robots, Genova, pp. 308–313 (2006)
5. Hashimoto, T., Hitramatsu, S., Tsuji, T., Kobayashi, H.: Development of the face robot SAYA for rich facial expressions. In: Proceeding of SICECICASE International Joint Conference, Busan, pp. 5423–5428 (2006)
6. Nori, F., Jamone, L., Metta, G., Sandini, G.: Accurate control of a human-like tendon-driven neck. In: Procedings of IEEE International Conference on Humanoid Robots, Pittsburgh, Pennsylvania, USA, pp. 371–378 (2007)
7. Jiri, T., John, Z., Shannon, R.: Fundamental comparison of the use of serial and parallel kinematics for machines tools. Manuf. Technol. **48**(1), 351–356 (1999)
8. Gao, B., Xu, J., Zhao, J., Xi, N., Shen, Y., Yang, R.: A Humanoid neck system featuring low motion noise. J. Intell. Robot. Syst. **67**(2), 101–106 (2012)

9. Gao, B., Xu, J., Zhao, J., Xi, N.: Combined inverse kinematic and static analysis and optimal design of a cable-driven mechanism with a spring spine. Adv. Robot. **26**(8-9), 923–946 (2012)
10. Gao, B., Song, H., Zhao, J., Guo, S., Sun, L., Tang, Y.: Inverse kinematics and workspace analysis of a cable-driven parallel robot with a spring spine. Mech. Mach. Theory **76**, 56–69 (2014)
11. Sapra, R., Mathew, M.J., Majumder, S.: A Solution to inverse kinematics problem using the concept of sampling importance resampling. In: 2014 Fourth International Conference on Advanced Computing & Communication Technologies, pp. 471-477. Rohtak, India (2014)
12. Kucuk, S., Bingul, Z.: Robot kinematics: forward and inverse kinematics. In: Cubero, S. (ed.) Industrial Robotics: Theory, Modelling and Control, pp. 117–147. InTech, Rijeka, Croatia (2006)
13. Chen, I.M., Yang, G., Kang, I.G.: Numerical inverse kinematics for modular reconfigurable robots. J. Robot. Syst. **16**(4), 213–225 (1999)
14. Gregory, S.C.: A general numerical method for hyper-redundant manipulator inverse kinematics. In: IEEE International Conference on Robotics and Automation, pp. 107-112. Atlanta, USA (1993)
15. Kallmann, M.: Analytical inverse kinematics with body posture control. Comput. Anim. Virtual Worlds **19**(2), 79–91 (2008)
16. Kofinas, N., Orfanoudakis, E., Lagoudakis, M.G.: Complete analytical inverse kinematics for NAO. In: 13th International Conference on Autonomous Robot Systems, pp. 1–6. Lisbon, Portuguesa (2013)
17. Verhoeven, R.: Analysis of the workspace of tendon-based stewart platforms. Ph.D. Thesis, University of Gerhard-Mercator, Duisburg, Germany (2004)
18. Zi, B., Duan, B., Du, J., Bao, H.: Dynamic modeling and active control of a cable suspended parallel robot. Mechatronics **18**(1), 1–12 (2008)
19. Lee, C., Ziegler, M.: A geometric approach in solving the inverse kinematics of PUMA robots. IEEE Trans. Aerosp. Electron. Syst. **20**(6), 695–706 (1984)
20. Li, S., Wang, Y., Chen, Q., Hu, W.: A new geometrical method for the inverse kinematics of the hyper-redundant manipulators. In: IEEE International Conference on Robotics and Biomimetics, pp. 1356–1359. Kunming, China (2006)
21. Neppalli, S., Matthew, A.C., Jones, B.A., Walker, I.: A geometrical approach to inverse kinematics for continuum manipulators. In: IEEERSJ International Conference on Intelligent Robots and Systems, pp. 3565–3570. Nice, France (2008)
22. Parker, J.K., Khoogar, A.R., Goldberg, D.K.: Inverse kinematics of redundant robots using genetic algorithms. In: IEEE International Conference on Robotics and Automation, pp. 271–276. Scottsdale, USA (1989)
23. Tabandeh, S., Clark, C., Melek, W.: A genetic algorithm approach to solve for multiple solutions of inverse kinematics using adaptive niching and clustering. In: IEEE Congress on Evolutionary Computation, pp. 1815–1822. Vancouver, Canada (2006)
24. Aydin, Y., Kucuk, S.: Quaternion based inverse kinematics for industrial robot manipulators with euler wrist. In: IEEE Congress on Mechatronics, pp. 581–586. Budapest, Hungary (2006)
25. Qiao, S., Liao, Q.: Inverse kinematic analysis of the general 6R serial manipulators based on double quaternions. Mech. Mach. Theory **45**(2), 193–199 (2010)
26. Guez, A., Ahmad, Z.: Solution to the inverse kinematics problem in robotics by neural networks. In: IEEE International Conference on Neural Networks, pp. 617–624. USA, San Diego (2013)
27. Ananthanarayanan, H., Ordonez, R.: Real-time inverse kinematics of redundant manipulator using a hybrid (analytical and numerical) method. In: IEEE International Conference on Advanced Robotics, pp. 1–6. Montevideo, Uruguay (2013)
28. Gao, B., Hu, J., Guo, S., Li, W., Kan, Q.: Lateral bending models of spring spine for cable-driven parallel mechanism. In: 11th World Congress on Intelligent Control and Automation, pp. 3176–3180. Shenyang, China (2014)

Bingtuan Gao received his B.E degree in Electrical Engineering and Automation, M.E. degree in Control Theory and Control Engineering, and Ph.D Degree in Power Electronics and Electrical Drive, from Harbin Institute of Technology, Harbin, China, in 2002, 2004, and 2007, respectively. From 2008 to 2010, he was a Post-doctor at the Department of Electrical and Computer Engineering, Michigan State University, East Lansing, USA. He is currently a professor at School of Electrical Engineering, Southeast University, Nanjing, China. His research interests include robotics, modeling and control of dynamic systems, renewable energy systems and smart grids.

Zhenyu Zhu received his B.E degree in Electrical Engineering and Automation from Southeast University, Nanjing, China, in 2015. He is currently a postgraduate student at School of Electrical Engineering, Southeast University, Nanjing, China. His research interests include robotics and power demand side management.

Jianguo Zhao received the B.E. degree in Mechanical Engineering from Harbin Institute of Technology, Harbin, China and M.E. degree in Mechatronic Engineering from Shenzhen Graduate School, Harbin Institute of Technology, Shenzhen, China. He received his PhD degree in Electrical Engineering from Michigan State University, East Lansing, Michigan, USA. He is currently an Assistant Professor at Colorado State University. His research interests include bio-inspired robotics, dynamics and control, and vision based control.

Leijie Jiang received the B.E. degree in Electrical Engineering and Automation from Yangzhou University, Yangzhou, China, in 2011 and the M.E. degree in Mechatronic Engineering from Xi'an Polytechnic University, Xi'an, China, in 2014. He is currently working toward the Ph.D. degree with the School of Electrical Engineering, Southeast University, Nanjing, China. His research interests include motor drive, intelligent control and system, and robotics.